

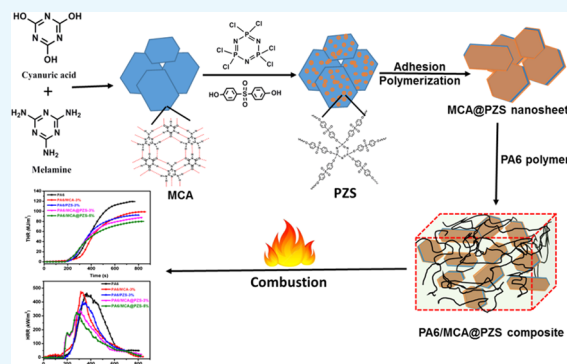
Thermal Stability, Pyrolysis Behavior, and Fire-Retardant Performance of Melamine Cyanurate@Poly(cyclotriphosphazene-co-4,4'-sulfonyl diphenol) Hybrid Nanosheet-Containing Polyamide 6 Composites

Kuruma Malkappa[†] and Suprakas Sinha Ray^{*,†,‡,§}

[†]DST-CSIR National Centre for Nanostructured Materials, Council for Scientific and Industrial Research, Pretoria 0001, South Africa

[‡]Department of Applied Chemistry, University of Johannesburg, Doornfontein, 2028 Johannesburg, South Africa

ABSTRACT: A novel halogen-free highly cross-linked supramolecular poly(cyclotriphosphazene-co-4,4'-sulfonyl diphenol) (PZS)-functionalized melamine cyanurate (MCA) (MCA@PZS) hybrid nanosheet fire-retardant (FR) was synthesized and thoroughly characterized using scanning electron microscopy, Fourier-transform infrared (FTIR), X-ray diffraction, and X-ray photoelectron spectroscopy analyses. The polyamide 6 (PA6) composites comprising MCA, PZS, and the MCA@PZS hybrids were prepared via the melt-blending technique. The thermogravimetric analysis combined with FTIR and mass spectroscopy revealed that during thermal degradation, the PA6/MCA@PZS composites released less toxic gases and small organic volatile compounds than the neat PA6 and composites containing MCA or PZS solely. Moreover, compared to neat PA6, the PA6 composite with a 5 wt % MCA@PZS hybrid exhibited enhanced fire retardation properties, with a 29.4 and 32.1% decrease in the peak heat and total heat release rates, respectively. Besides, the PA6 composites with MCA@PZS-5% content achieved a V-0 rating in the UL-94 test. Finally, based on the obtained results from gaseous and condensed phases, the possible mechanism responsible for improved FR properties of the PA6/MCA@PZS composites was proposed.



1. INTRODUCTION

Polyamide 6 (PA6), a vital engineering polymer, has attracted considerable attention in many fields of applications because of its excellent mechanical properties, abrasion resistance, self-lubrication ability, electrical properties, chemical corrosion resistance, and oil-proof performance.^{1,2} However, the inherent flammability of PA6 has restricted its applications, particularly in electrical and electronic products. To decrease its flammability PA6 is generally compounded with halogenated fire-retardants (FRs). However, the use of such FRs leads to the release of dense smoke and toxic gases. Thus, because of environmental issues, there is a strong desire to replace halogenated FRs with halogen-free alternatives that are currently available in the FR market. The ecological problem has led to extensive research on ways to increase the fire safety of PA6 polymers by introducing halogen-free FRs such as melamine derivatives,^{3–5} phosphorous-based compounds,⁶ polyphosphazenes,^{7,8} and a combination of P,N-based intumescent FRs.^{9,10}

Melamine cyanurate (MCA) is another environmentally friendly nitrogen-based FR that contains a planar network structure with hydrogen bonds between the melamine and cyanuric acid.¹¹ In this direction, Hu et al.³ prepared PA6

composites with different MCA contents and reported that a composite comprising 15 wt % MCA is required to achieve a V-0 rating in the UL-94 test. Thus, to increase the efficiency of the FR activity and decrease the loading percentage, surface functionalization with other FR compounds must be performed. Tao and Li¹² functionalized various types of bases onto the MCA surface and used the products in the PA6 composites. They observed that PA6 composites comprising cytosine-functionalized MCA presented better FR activity because of their high surface area, which accelerates PA6 degradation to form cross-linked char. Wu et al.⁵ synthesized PA6/MCA composites via in situ polymerization and observed that the composite comprising 6.8 wt % MCA exhibited excellent mechanical and flammability properties with a V-0 rating in the UL-94 test. The uniform dispersion of the MCA nanoparticles in the polymer matrix was responsible for excellent fire properties.^{13,14} Feng et al.¹⁵ prepared PA6 composites with melamine (M)/MoS₂ and MCA/MoS₂ and observed that MCA/MoS₂ displayed better FR activity because

Received: February 6, 2019

Accepted: March 18, 2019

Published: June 3, 2019

Scheme 1. Schematic Model for the Formation of Highly Cross-Linked Supramolecular PZS-Functionalized MCA (MCA@PZS) Hybrid Nanosheets

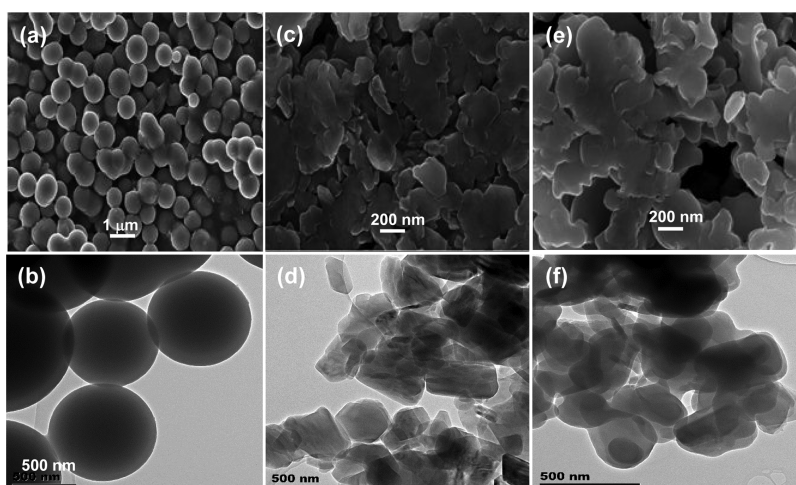
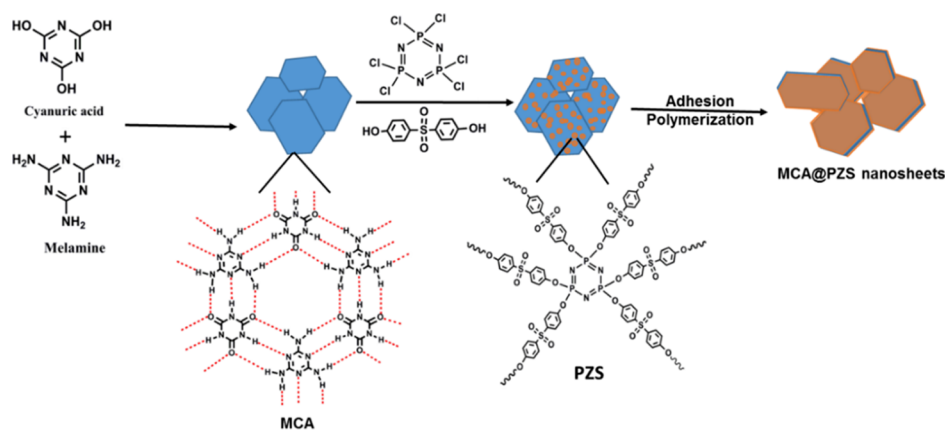


Figure 1. Respective field emission-SEM (FE-SEM) and TEM images of (a,b) the synthesized PZS, (c,d) MCA, and (e,f) MCA@PZS hybrid.

of the synergetic effect between the MCA and MoS₂. The melamine derivatives and MCA were as synergetic agents for phosphorous-based FR polymers, particularly P–N-containing FR compounds, which exhibited promising improvement.^{16–18}

Recently, cyclotriphosphazene derivatives showed excellent reactivity and high P- and N-contents, which play an essential role in the development of the thermal and flammability properties of the polymers, such as polyurethane,¹⁹ polylactide,^{19,20} and unsaturated polyester.²¹ Mainly, poly(cyclotriphosphazene-co-4,4'-sulfonyl diphenol) (PZS) was employed for the surface functionalization of various nanomaterials through covalent and noncovalent bonds. The resulting hybrid nanomaterials provided better structural controllability with an alternate –P=N– units and improved the flammability, thermal conductivity, and other required properties of the composite.^{22–24} For example, boron nitride sheets coated with poly(phosphazene-co-bisphenol A) were synthesized and used in epoxy resins. The resulting composites exhibited immediate improvement in both the thermal stability and electrical conductivity.²⁴ However, few papers on the use of polyphosphazene nanomaterials as FRs and their combination with other FRs to further increase the fire retardancy of polymer materials have been reported to date.^{25,26}

Accordingly, this paper reports the synthesis of a PZS-functionalized MCA (MCA@PZS) hybrid using planar MCA nanosheets as a template to achieve adequate FR activity. The

resulting novel supramolecular MCA@PZS hybrid, which was highly cross-linked because of its high P-, N- and S-contents, was then used to prepare PA6 composites with different MCA@PZS hybrid weight percentages, including individual MCA and PZS. The thermal stability of PA6 and various composites were studied using a thermogravimetric analyzer, and the toxic gas evolution behavior of the PA6 composites was investigated by thermogravimetric analysis (TGA)–Fourier-transform infrared (TG–FTIR)–mass spectrometry (MS) and pyrolysis gas chromatography (Py–GC)–MS. Subsequently, the FR activity of the resulting PA6 composites was analyzed by cone calorimetry and UL-94 testing. Moreover, time-dependence melt-state rheology was used to understand the cross-linking behavior of PA6 and its composites. Finally, microscopic analysis of the char residues completed the study of the FR activity.

2. RESULTS AND DISCUSSION

2.1. Synthesis and Characterization of the Supramolecular MCA@PZS Hybrid Nanosheets.

Scheme 1 presents the synthetic procedure and formation mechanism of the supramolecular MCA@PZS hybrid. The high polar solvent dimethyl sulfoxide (DMSO) was used to synthesize the MCA nanosheets. This solvent favored the formation of extensive H-bonding between melamine and cyanuric acid, thereby improving the supramolecular structure during the

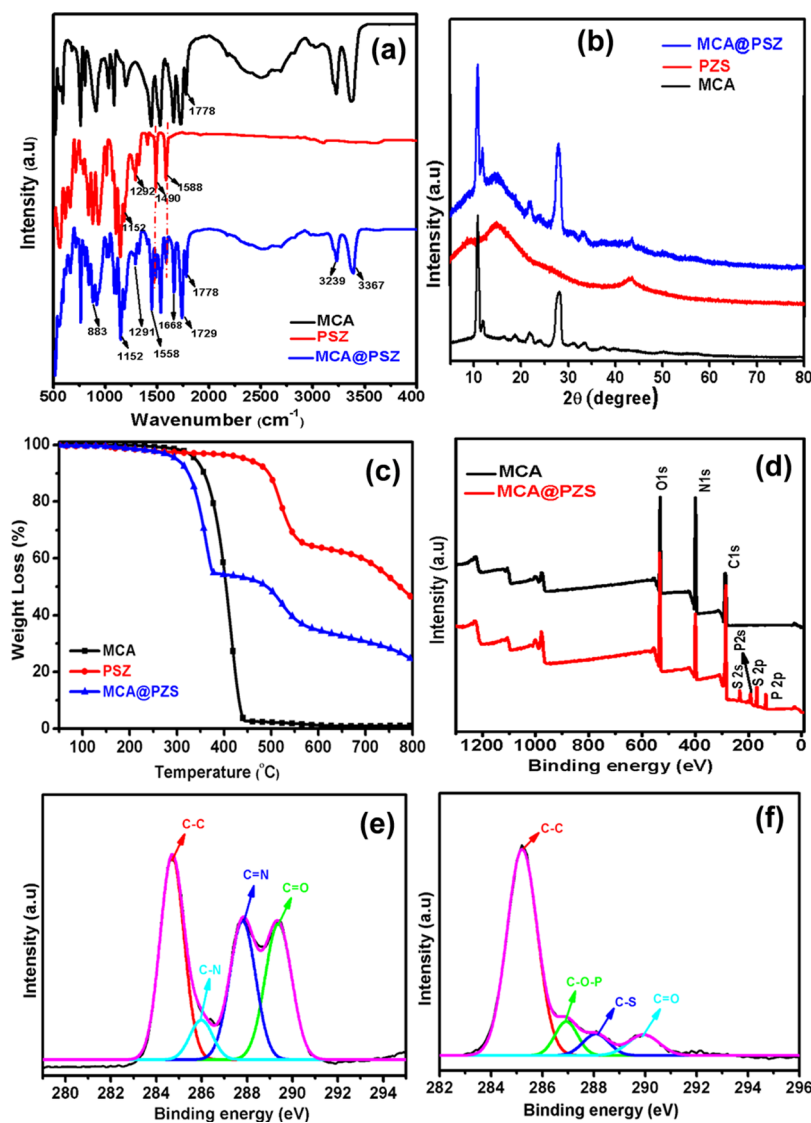


Figure 2. (a) FTIR spectra, (b) powder XRD patterns, (c) TGA data, and (d) XPS plots of MCA, PZS, and the MCA@PZS hybrid; high-resolution C 1s spectra of (e) MCA and (f) the MCA@PZS hybrid.

self-assembly process (Scheme 1). For the synthesis of the supramolecular MCA@PZS hybrid, the MCA nanosheets acted as a hard template for the growth of the PZS nucleus on the substrate. The synthetic procedure followed the absorption and polymerization mechanism previously reported for oligomeric species.^{27–35} Thus, the polymerization between hexachlorocyclo-triphosphazenes (HCCPs) and 4,4'-dihydroxydiphenyl sulfone (BPS) in the presence of triethylamine (TEA) primarily proceeded via the generation of the PZS nucleus on the surface of the MCA nanosheets along with the release of HCl as a by-product. This by-product was then recaptured by TEA, thereby accelerating the polymerization reaction until the polymerization of HCCP and BPS was completed. In the initial stage of the reaction, the formed PZS nuclei were unstable and could easily adhere onto the surface of the MCA nanosheets. These nuclei then aggregated with each other, possibly via H-bonding, to form stable particles. Subsequently, adhesion polymerization was conducted sequentially to coat the P,N-containing highly cross-linked PZS evenly across the whole surface of the MCA nanosheet. Scheme 1 also presents the approaching method.

To confirm the morphology of the successfully synthesized products, the structure of the supramolecular MCA@PZS hybrid together with those of MCA and PZS were investigated by scanning electron microscopy (SEM) and transmission electron microscopy (TEM) (Figure 1). The micrographs revealed that PZS formed as microspheres [Figure 1a,b], whereas MCA displayed a nanosheet morphology [Figure 1c,d]. The SEM and TEM images of the MCA@PZS hybrid [Figure 1e,f] clearly illustrated that after the PZS was functionalized onto the surface of the MCA nanosheets, the surface became relatively smooth. Moreover, the absence of separate PZS microspheres indicated that the MCA nanosheets were uniformly functionalized by PZS. Finally, FTIR, X-ray diffraction (XRD), and X-ray photoelectron spectroscopy (XPS) experiments were performed to further confirm the formation and structure of the MCA@PZS hybrid.

The FTIR spectra of MCA, PZS, and MCA@PZS [Figure 2a] confirmed the formation of the supramolecular MCA@PZS hybrid through condensed polymerization from the respective monomers. The main characteristic peaks of the MCA spectrum, at 3239 and 3367 cm^{-1} , were assigned to the

symmetric and asymmetric absorption of the $-\text{NH}-$ and $-\text{NH}_2$ groups,³⁶ respectively, those at 1778 and 1729 cm^{-1} corresponded to the $-\text{C}=\text{O}$ group, and the peak at 1668 cm^{-1} was assigned to the $-\text{C}=\text{N}$ group. The PZS-coated MCA nanosheets showed some additional absorption peaks: the firm absorption peaks at 1152 and 883 cm^{-1} , assigned to the $\text{P}=\text{N}$ and $\text{P}-\text{N}$ groups, respectively,³⁷ are the main characteristic absorption peaks of cyclotriphosphazene. The characteristic absorption peaks at 1291 and 1152 cm^{-1} were assigned to the $\text{O}=\text{S}=\text{O}$ group of BPS, whereas the peaks at 1490 and 1588 cm^{-1} were assigned to the phenyl group from BPS absorption.³⁸ Hence, these data indicated that PZS was successfully functionalized over the entire surface of the MCA nanosheets.

XRD analysis of all the samples [Figure 2b] was also performed to support the above results further. The MCA XRD pattern [Figure 2b] indicated crystallinity with 2θ peaks at the lower angle side (10.67, 18.56, and 21.45°) corresponding to the (100), (110), and (200) planes, respectively, thereby supporting the in-plane hexagonal structure of the channels. Additionally, the XRD peak at 27.90° was attributed to the presence of the assembled individual 2D nanosheets and was similar to the data observed for graphite. The amorphous nature of PZS was responsible for the broad peak at $2\theta \approx 15^\circ$. Figure 2b reveals that the XRD pattern of the MCA@PZS hybrid contains a broad amorphous peak at $2\theta = 15^\circ$, together with all the characteristic peaks of the MCA nanosheets, which corresponds to the amorphous PZS phase and demonstrates the effective functionalization of PZS on the surface of the MCA nanosheets.

TGA evaluated the thermal stabilities of PZS, MCA, and the MCA@PZS hybrid under nitrogen atmosphere [Figure 2c]. The two critical temperatures necessary to analyze the thermal properties of a substance are the onset (T_{onset}) and maximum (T_{max}) degradation temperatures, defined as the temperatures at 5% and maximum weight loss, respectively. MCA displayed a maximum weight loss in the temperature range 300–400 °C because of the formation of the cross-linked melamine derivatives melam, melem, and melon with the elimination of NH_3 ; this is in good agreement with previously reported data.³⁹ Figure 2c reveals that the T_{onset} value of MCA is approximately 370 °C and that the char residue at 800 °C is 1.2%.

On the other hand, the T_{onset} value of PZS is 480 °C, whereas its char residue at 800 °C is 52%. These values revealed that PZS displays superior thermal stability over MCA. However, PZS functionalization of the MCA surface improved the thermal stability of MCA@PZS and the hybrid exhibited a combination of the thermal behavior of MCA and PZS [Figure 2c]. The T_{onset} value of the MCA@PZS hybrid was lower than that of MCA because the presence of PZS accelerated the degradation of MCA at an early stage and improved its char residue (32%) over that of MCA by approximately 31%. From the TGA curve of the MCA@PZS hybrid [Figure 2c], 31% PZS was functionalized on the surface of the MCA nanosheets. XPS provided diversified information on the surface composition and chemical states of MCA and the MCA@PZS hybrid and thus, clear information about their chemical structure and composition. The XPS spectra of MCA and the MCA@PZS hybrid are displayed in Figure 2d, whereas the high-resolution images of the C 1s XPS spectra of MCA and the MCA@PZS hybrid are presented in Figure 2e,f, respectively. The data revealed that the surface of the MCA

nanosheets is composed of C, N, and O. The data in Figure 2d also showed that along with these three elements, the XPS spectra of the MCA@PZS hybrid also contained P and S peaks obtained from PZS. Also, in the case of the MCA@PZS hybrid, the intensities of C 1s and O 1s were increased, whereas the intensity of the N 1s peak was decreased when compared to those of MCA. This changes in relevant peak intensities and elemental composition confirmed that the PZS functionalized onto the surface of the MCA nanosheets.⁴⁰ The high-resolution C 1s spectrum of MCA [Figure 2e] confirms the presence of C–C (284.6 eV), C–N (286.0 eV), C=N (288.1 eV), and C=O (289.6 eV) groups. After PZS functionalization on the MCA surface, the C 1s spectrum of the MCA@PZS hybrid [Figure 2f] showed two additional peaks, assigned to the C–O–P (286.5 eV) and C–S (287.3 eV) groups, which correspond to the PZS peaks.^{41,42} These data also clearly indicated that the PZS functionalized onto the surface of the MCA nanosheets.

2.2. Thermal Stability of PA6 and Its Composites.

TGA evaluated the thermal stability of neat PA6 and its composites under nitrogen and air atmospheres. Figure 3

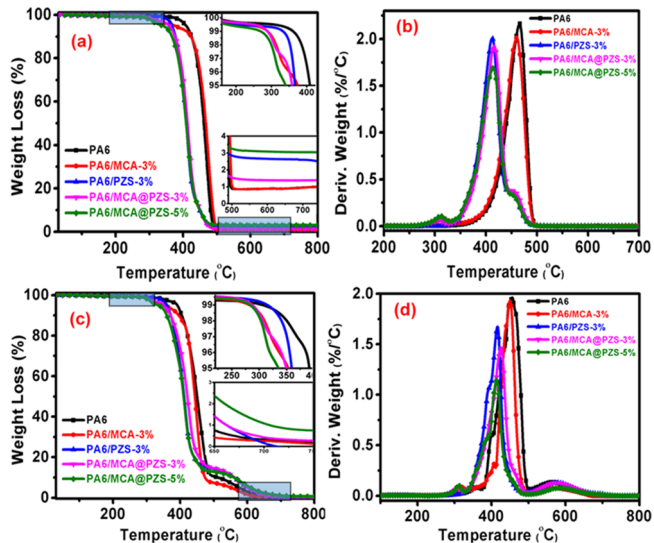


Figure 3. TGA and derivative thermogravimetric (DTG) curves of PA6, PA6/MCA-3%, PA6/PZS-3%, PA6/MCA@PZS-3%, and PA6/MCA@PZS-5% in (a,b) N_2 atmosphere and (c,d) air atmosphere.

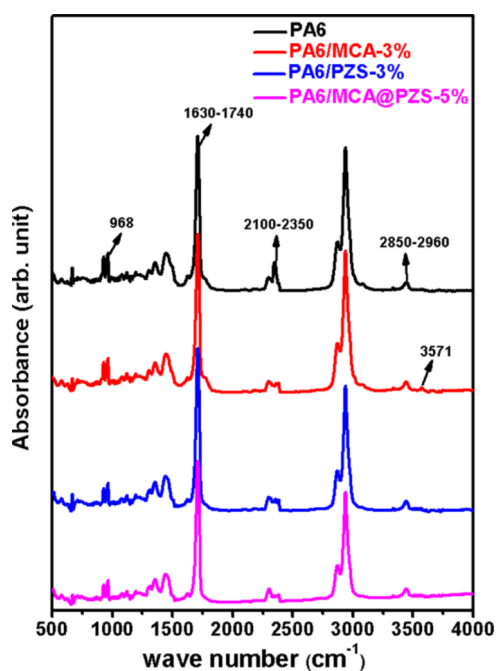
presents the TGA results, and Table 1 summarizes the relevant data calculated from TGA thermograms. In both atmospheric conditions, all samples follow similar decomposition paths except early stage degradation. In a nitrogen environment [Figure 3a], all the samples displayed typical single-stage degradation in the temperature range of 380–515 °C, corresponding to the degradation of neat PA6. On the other hand, in air atmosphere [Figure 3c], all the TGA plots displayed typical second-stage degradation (typical temperature range: 480–540 °C), which might be linked with the oxidation and aromatization of aliphatic carbons followed by the release of CO and CO_2 gases. In an air atmosphere, the first stage degradation is more significant because of the oxidative degradation of unstable char. The temperature at 5 wt % weight loss (T_{onset}), 80 wt % weight loss (T_{max}), and the residual char percentages at 800 °C are also listed in Table 1, to compare the thermal degradation behavior of neat PA6 and various PA6 composites. The T_{onset} and T_{max} for PA6 are

Table 1. Data Calculated from TGA and DTG Curves of PA6, PA6/MCA-3%, PA6/PZS-3%, PA6/MCA@PZS-3%, and PA6/MCA@PZS-5% in N₂ Atmosphere and Air Atmosphere

samples	N ₂ atmosphere				O ₂ atmosphere			
	T_{onset} (°C)	T_{max} (°C)	char at 800 °C (%)	α_{max} (%/°C)	T_{onset} (°C)	T_{max} (°C)	char at 800 °C (%)	α_{max} (%/°C)
PA6	411.1	465.5	1.0	2.2	391.4	455.9	0.14	1.96
PA6/MCA-3%	372.9	460.2	1.0	1.9	349.0	450.4	0.09	1.93
PA6/PZS-3%	365.6	412.4	2.1	2.0	353.8	415.3	0.17	1.67
PA6/MCA@PZS-3%	360.4	415.5	1.6	1.9	350.0	417.8	0.15	1.45
PA6/MCA@PZS-5%	337.4	412.3	3.1	1.5	328.0	413.3	0.85	1.16

411.06 and 465.53 °C, respectively. In the case of composites in both atmospheres, compared to neat PA6, the initial stability of all composites decreased, which is a common observation for FR-containing polymer composites because FR accelerates the polymer matrix degradation in an early stage to improve the residual char formation.¹³ The T_{onset} for PA6/MCA-3% and PA6/PZS-3% composites are 372.95 and 365.62 °C, respectively. On the other hand, in the case of PA6/MCA@PZS composites, the early stage thermal stability decreased, and this trend becomes stronger with increasing MCA@PZS hybrid nanosheets' loading in the composite; for example, for PA6/MCA@PZS-5%, the T_{onset} is 337.44 °C. For the derivate plots [Figure 3b,d] shows that the maximum weight loss rate is higher in PA6 composites than in the neat PA6 and this is more prominent in the air atmosphere. In the case of PA6/MCA@PZS composites with increasing MCA@PZS loading in the PA6 matrix, the peak intensity decreased. Such an observation supports that the MCA@PZS hybrid promotes PA6 matrix degradation in the early stage to quickly form a thermally insulating char, which provides strong protection to the underlying material against further degradation at the high-temperature range. Furthermore, in the case of PA6/MCA@PZS composites, the data calculated from TGA thermograms (Table 1) show that the residual char yield at 800 °C is higher in the nitrogen atmosphere than in air, and this yield also increases with the increased loading of MCA@PZS in the composites.

2.3. Volatile Gaseous Products of PA6 and Various PA6 Composites Analyzed by TG–FTIR–MS. When a polymer material is associated with FR activity, it is important to analyze the emitted volatile components during thermal degradation. The TG–FTIR is an important technique which was used to evaluate the effect of the FR compounds (MCA and PZS) and the MCA@PZS hybrid on the released gas components of PA6 during thermal degradation. Figure 4 presents the resulting FTIR spectra of the neat PA6 and its composites with different FR contents at the maximum decomposition stage. The spectra indicated that except for the small difference in the intensities of the released pyrolytic components and toxic gases, the thermal degradation behavior of PA6 and its composites with FR are near identical. On the basis of the FTIR absorption bands, some of the released pyrolytic components were identified as hydrocarbons (2960 cm⁻¹), aromatic compounds (1640 cm⁻¹), carbonyl compounds (1730 cm⁻¹), CO (2138 cm⁻¹), CO₂ (2346 cm⁻¹), and NH₃ (968 cm⁻¹).⁴³ Figure 5 reports the Gram–Schmidt plots (a) and plots of the released volatile components [(b) CO, (c) CO₂, and (d) NH₃] versus time. These plots revealed that the absorbance intensity of the released volatile components was relatively lower in the presence of an FR. Moreover, the absorbance intensity of the MCA@PZS hybrid was significantly less than those of MCA and PZS. The

**Figure 4.** FTIR spectra of neat PA6 and its composites with different FR contents at the maximum decomposition stage.

significantly decreased absorbance intensity was attributed to the MCA@PZS hybrid nanosheets, which promote char formation and strengthen the char structure because of the formation of highly cross-linked components, thereby decreasing the thermal decomposition and gas diffusion rates. The maximum absorbance intensities of the released volatile components declined to approximately 60% of the intensities of the volatile components released by pure PA6, which indicated that the amount of volatiles released from the PA6/MCA@PZS-5% composite was much lower than that released from pure PA6. Volatile organic compounds generate smoke upon condensation. Hence, a decrease in the amount of released volatiles would result in a decrease in fire toxicity and smoke.

To evaluate the pyrolysis mechanism of various samples, the Py–GC–MS spectra of PA6, PA6/MCA-3%, and PA6/MCA@PZS-5% were recorded, and the results are reported in Figure 6. Figure 7 indicates the proposed possible pyrolysis mechanisms.^{44–46} The pyrolysis temperature was considered as the temperature at which the samples were completely decomposed. Generally, the thermal degradation of PA6 leads to many different products with caprolactam ($m/z = 113$) as the main degradation product.^{47,48} The apparent fragment peaks at $m/z = 94$ and 93 correspond to the phenol and phenoxyl groups, respectively. Subsequently, the phenol decomposed and new fragmented peaks at m/z (m , mass; z ,

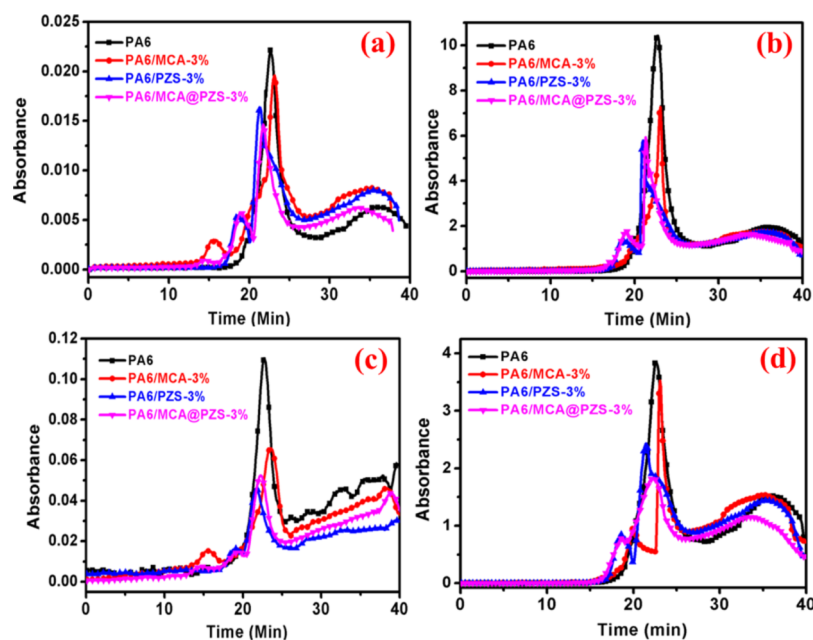


Figure 5. Absorbance spectra of the pyrolysis products from PA6, PA6/MCA-3%, PA6/PZS-3%, and PA6/MCA@PZS-5%. (a) Gram–Schmidt plots and plots of the released volatile components versus time: (b) CO, (c) CO₂, and (d) NH₃.

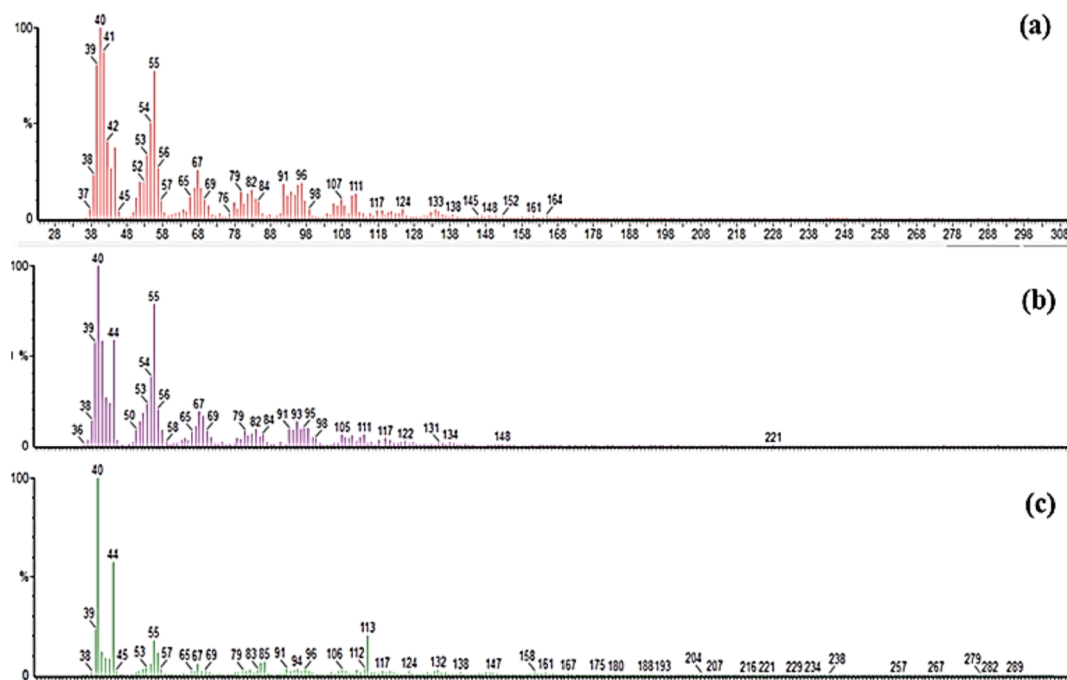


Figure 6. Mass spectra of (a) PA6, (b) PA6/MCA-3%, and (c) the PA6/MCA@PZS-5% composite at the maximum degradation stage.

charge number of ions) = 80, 79, 66, 53, and 40 were observed. Similarly, the released few pyrolysis components were identified based on their m/z values, and Table 2 presents their chemical structures. The degradation process that occurred in the presence of MCA and the MCA@PZS hybrid was utterly different to that observed for the neat PA6.

Moreover, the PA6/MCA@PZS-5% composite presented a significant decrease in the peak intensities and eluted total small volatile organic compounds over those seen for the PA6/MCA-3% composite (Figure 6). These results clearly indicate that the presence of the MCA@PZS hybrid improved the FR activity of PA6 because of the formation of highly cross-linked

products during thermal degradation (Figure 7) and significantly decreased the release of small volatile organic compounds compared to those released by neat PA6. The data in Table 2 clearly illustrate that the released volatiles comprise benzene and its derivatives, heteroatom-containing cyclic compounds, and various other small volatile oligomeric organic compounds that are responsible for causing secondary injury. Moreover, all these compounds form dense smoke upon condensation, which can reduce visibility and increase the difficulty of fire rescue.⁴⁹ Notably, the pyrolysis compounds released from the PA6/MCA@PZS composites during thermal degradation did not include phosphorus-containing com-

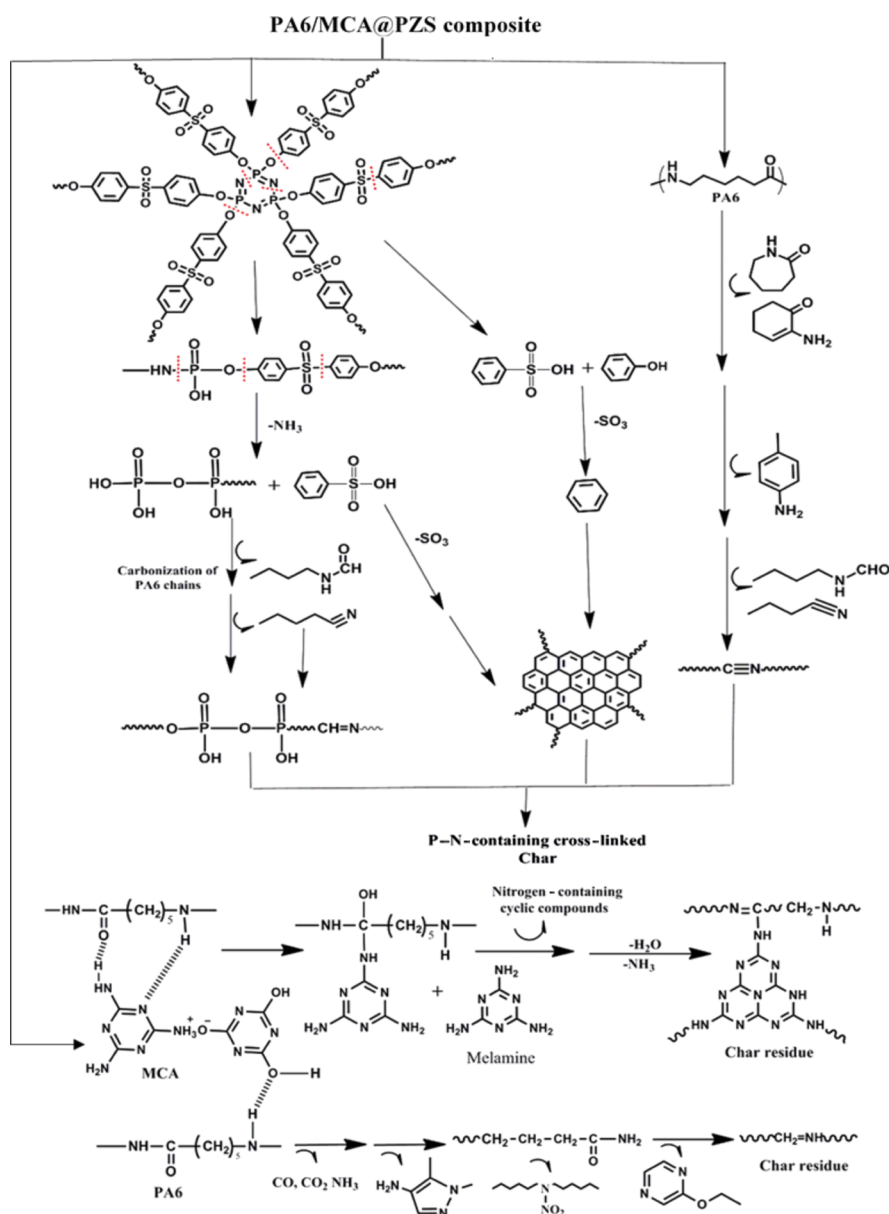


Figure 7. Proposed possible thermal degradation mechanism of the PA6/MCA@PZS composite during combustion. At the high-temperature range, the MCA and PZS interact with PA6 degraded components in different paths with the release of nonflammable gases and various nitrogen-based small volatile components. The PZS part mainly involves during dehydration of polymer chains to form an insulating char through the formation of phosphoric acids, pyro-phosphoric acids, etc. The MCA exhibits the flame-retardant action through endothermic degradation and release of nonflammable gases through the creation of condensed compounds of melamine-derivatives.


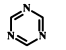
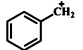
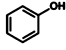
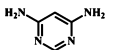
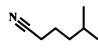
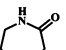
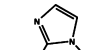

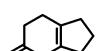
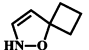
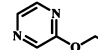
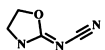
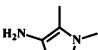
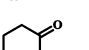
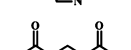
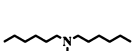
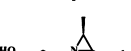
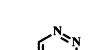
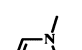
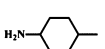
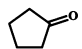
pounds, indicating that cyclotriphosphazenes are entirely involved in the cross-linked char residue formation.⁵⁰ Hence, PA6/MCA@PZS-5% composites exhibited high FR activity over the individual MCA and PZS.

To understand the degradation and cross-linking characteristics, the melt-state rheological experiments of neat PA6 and various composites were carried out at 200 °C in air atmosphere.⁴⁹ Figure 8 reports the time-dependence storage modulus (G'), loss modulus (G''), and complex viscosity (η^*) of various samples. The results clearly show that the presence of the MCA@PZS hybrid improved the rheological properties (G' , G'' , and η^*) of PA6/MCA@PZS composites over time as compared to individual MCA- or PZS-containing composites. Moreover, increasing the MCA@PZS loading in the composite further improves the rheological properties. Because of its

combined effect of MCA and PZS and it involved in different directions with releasing of nonflammable gases and formed crosslinked compounds^{50,51} during combustion as shown in Figure 7. Hence, the composite containing MCA@PZS hybrid forms cross-linked P-N-containing char during combustion, which provides strong barrier properties to inhibit the evolution of heat and toxic gases.

2.4. Fire Properties and Analysis of the Char Residue of PA6 and Its Composites. The fire performance of PA6 and its composites with various FR contents (MCA, PZS, and MCA@PZS hybrid) was next analyzed by cone calorimetry. The heat release rate (HRR), total heat release (THR), CO production (COP), and CO₂ production (CO₂P) versus time curves are displayed in Figure 9, whereas some of the essential parameter values [_pHRR, THR, COP, CO₂P, and maximum

Table 2. Small Organic Components Released during the Thermal Degradation of PA6 and Its Composites with Different FR Compounds^a

m/z	Structure	m/z	Structure
44	<chem>O=C=O</chem>	42	<chem>O=C=N^+</chem>
77		81	
91		94	
110		111	
113		124	
124		138	
178		132	
111		111	
111		144	
230		157	
112		100	
113		84	

^am, mass; z, charge number of ion.

average heat rate emission (MAHRE)] obtained from the flammability test are listed in Table 3. During polymer combustion, the fire intensity and spread rate mainly depend on the released HRR and thus, the most effective FR system always displays the lowest HRR values.^{13,14} Notably, the pure PA6 burned rapidly, with HRR and THR values of 453.4 kW/m² and 119.9 MJ/m², respectively. When 3 wt % MCA was incorporated into the PA6 matrix, the HRR value slightly increased to 471.5 kW/m², whereas the THR value was reduced to 99.1 MJ/m². The higher HRR peak value may be due to the formation of fractured (loosely bonded or un-cross-linked) char formation during the early stage of combustion.

On the other hand, the introduction of 3 wt % PZS into PA6 decreased both the HRR and THR values (397.8 kW/m² and 92.3 MJ/m², respectively). However, the data in Figure 9 and Table 3 reveal that the most significant decreases were observed for the PA6 composites comprising the MCA@PZS hybrid, with the PA6/MCA@PZS-5% composite exhibiting the lowest HRR and THR values (320.1 kW/m² and 80.2 MJ/m², respectively). This occurred because in the presence of a hybrid FR, the polymer degrades faster and forms a thermal insulating char with extensive P–N cross-linkage that protects the material from further substrate degradation at higher temperatures. CO is a very significant toxic gas that must be considered because when it combines with other toxic gases such as HCN it becomes highly toxic. Hence, the COP is also

an essential factor to evaluate the fire safety of polymers. It is also well known that cone calorimetry is based on the oxygen consumption principle so that the HRR of the burning polymer material is equivalent to oxygen consumption. Polymer combustion instantaneously releases heat radiation and some of the oxidized gases, including CO₂. Therefore, the CO₂P plots versus time exhibit similar trends to those observed in the HRR plots [Figure 9c]. The CO₂P and COP peaks for neat PA6 were determined as 340 and 1.9 mg/s, respectively [Figure 9c,d]. After adding 3 wt % MCA and PZS to PA6, a slight decrease in both values was observed.

On the other hand, the CO₂P and COP values for the PA6 composites comprising the MCA@PZS hybrid were significantly lower and the PA6/MCA@PZS-5% composite produced CO₂P and COP values of 240 and 1.45 mg/s, respectively. This was attributed to two main reasons: (i) the combined effect of MCA and PZS and (ii) the formation of a more compact dense char during combustion, which decreases the evolution of the small organic volatiles responsible for CO and CO₂P during further thermal oxidation. Table 3 illustrates that the MAHRE values of the composites comprising the MCA@PZS hybrid are significantly lower than those of the pure PA6; moreover, an increase in the MCA@PZS hybrid content of the PA6 composites further reduced the MAHRE values.

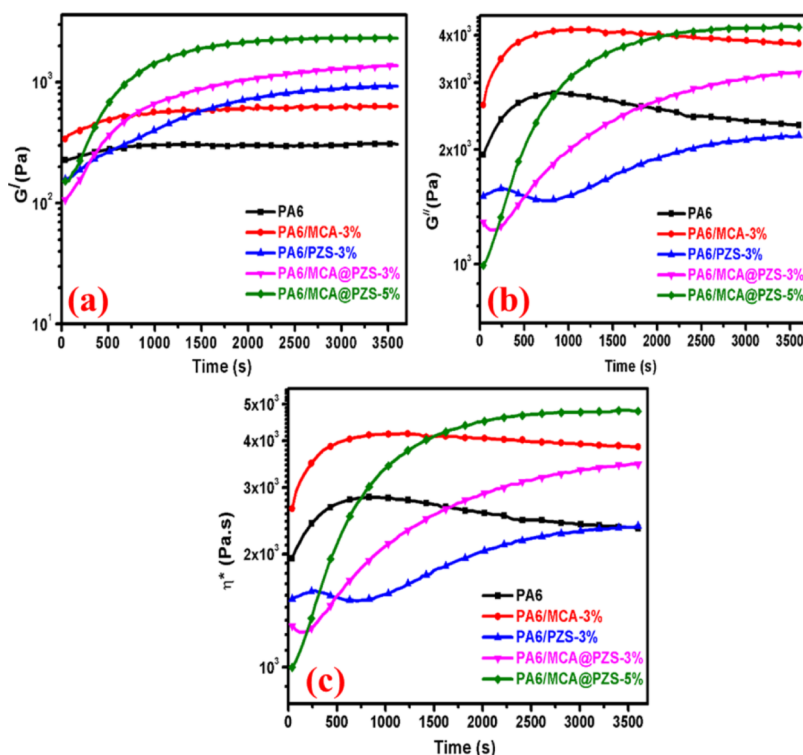


Figure 8. Time-dependence (measured at 200 °C in air atmosphere) (a) storage modulus (G'), (b) loss modulus (G''), and (c) complex viscosity (η^*) of neat PA6 and various composites.

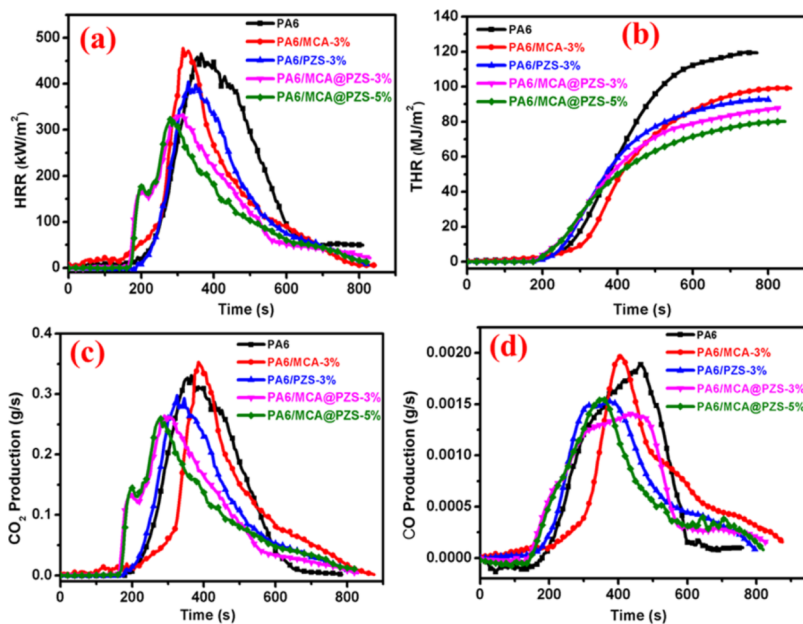


Figure 9. Cone calorimetry plots of PA6 and its composites with different FRs indicated in the figure: (a) HRR, (b) THR rate, (c) CO_2 P, and (d) COP vs time.

The complete analysis of the FR activity should include the char structure. Thus, the residual chars from the cone calorimetry tests were collected and their relevant microstructure morphologies investigated (Figure 10). When the neat PA6 polymer was burned vigorously (fire test), breaking char residues were observed [Figure 10a]. When 3 wt % MCA was added to PA6, the resulting composite burning improved the char residue [Figure 10c]. However, the residual char skeleton contained many cracks and voids caused by the

release of nonflammable gases from MCA degradation during combustion. The composite with the MCA@PZS hybrid formed continuous and high compact intumescent char [Figure 10e], indicating the combination effect of the MCA@PZS hybrid, whereby PZS facilitated the carbonization of the PA6 polymer chains, whereas MCA released the nonflammable gases. Figure 10b,d,f illustrates the microstructural SEM images of the external char residues from

Table 3. Cone Calorimetry and UL-94 Data of the PA6 Composite with Different FR Contents^a

sample	p_{HRR} (kW/m ²)	THR (MJ/m ²)	COP (mg/s)	CO ₂ P (mg/s)	MAHRE	t_1 (s)	t_2 (s)	melt dripping	UL-94 rating
PA6	453.4	119.9	1.90	340	160.1	18.8	20.3	Y	NR
PA6/MCA-3%	471.5	99.1	1.95	350	172.9	8.5	15.3	N	V-2
PA6/PZS-3%	397.8	92.3	1.53	300	148.5	11.9	13.2	N	V-2
PA6/MCA@PZS-3%	333.9	88.0	1.42	260	143.1	10.9	12.3	N	V-1
PA6/MCA@PZS-5%	320.1	80.2	1.45	240	118.9	3.9	2.6	N	V-0

^aMAHRE = maximum average heat rate emission.

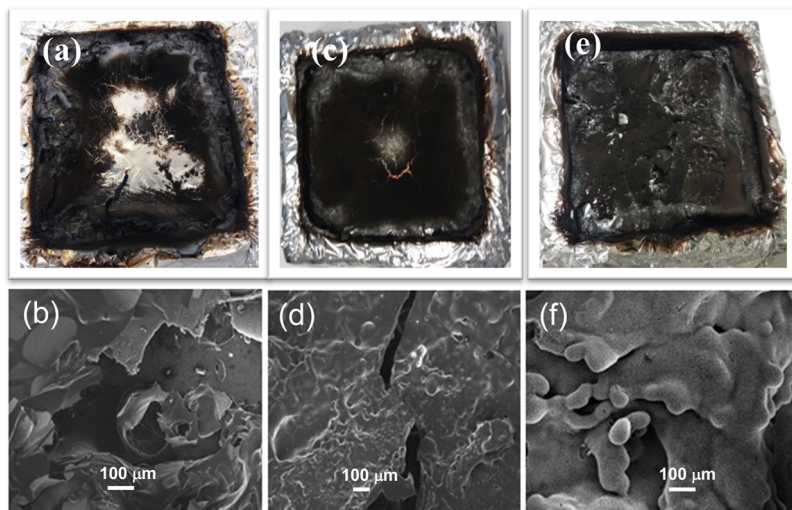


Figure 10. Respective digital photographs of the residual char from the cone calorimetry test and FE-SEM images of the char residues: (a,b) PA6, (c,d) PA6/MCA-3%, and (e,f) PA6/MCA@PZS-5%.

pure PA6 and the PA6/MCA-3% and PA6/MCA@PZS-5% composites.

For the neat PA6, the observed fragile and thin char pieces [Figure 10b] were due to the inferior quality of the char. Hence, in this case, strong char could not form on the surface of the substrate to prevent further degradation at the high-temperature conditions during combustion. As a result, the neat polymer burnt vigorously with strong melt drippings. Figure 10d shows the structural morphology of the residual char from PA6/MCA-3%. The image shows small bubbles on the surface and a broken char layer, which occurred because the char layers could not expand during combustion to inhibit the evolution of the volatile components. On the other hand, the char from the PA6/MCA@PZS-5% composite displayed a highly compact dense morphology [Figure 10f], attributed to the higher N- and P-contents in the MCA@PZS hybrid. Thus, during combustion, MCA and PZS interacted with the degraded PA6 components in different ways to form dense char containing extensive P–N cross-linkage. This form of char inhibits both mass and heat transfer as well as the release of volatile components (TG–FTIR and Py–GC–MS analysis sections). A more compact dense char layer with a micro-porous structure was also observed on the surface of the material. This type of char better blocks the gas and heat exchange between the fire zone area and the polymer material. Figure 10f illustrates the presence of bubbles on the surface of the char because of the inhibition of the release of the degraded volatile components and toxic gases. These results indicate that the MCA@PZS hybrid improved the fire safety of the polymer materials.

2.5. Flammability Rating—UL-94 Test. The FR activities of PA6 and its composites with different FRs were

evaluated by the UL-94 test and the results are also summarized in Table 3. The pure PA6 was highly flammable with strong melt drippings (Figure 11) and did not achieve a

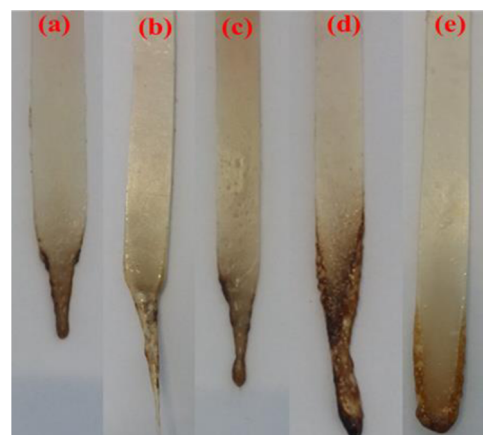


Figure 11. Photographs of specimen samples of PA6 composites after the UL-94 test: (a) PA6, (b) PA6/MCA-3%, (c) PA6/PZS-3%, (d) PA6/MCA@PZS-3%, and (e) PA6/MCA@PZS-5%. The digital pictures reported in this figure were taken by K.M. who is the first author of this work.

UL-94 rating. With the introduction of MCA into the PA6 matrix, a V-2 rating in the UL-94 test was attained.¹² The PA6 composite containing 3 wt % PZS decreased the burning time over that of neat PA6 and achieved a V-2 rating in the UL-94 test (Table 3).⁴⁹ On the other hand, the PA6 composites comprising the MCA@PZS hybrid brought significant changes in the flammability and the PA6/MCA@PZS-5% composite

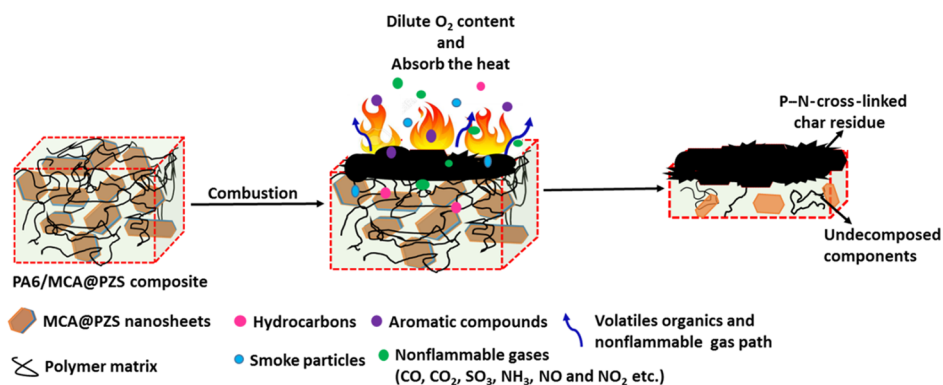


Figure 12. Schematic presentation of the proposed fire-retardant mechanism of the PA6/MCA@PZS composite. PA6, polyamide 6; MCA, melamine cyanurate; PZS, poly(cyclotriphosphazene-co-4,4'-sulfonyl diphenol).

exhibited a UL-94 V-0 rating. Overall, the MCA@PZS hybrid afforded a more substantial increase in the FR activity of the PA6 composites compared to those of the individual MCA and PZS. This may be due to the presence of higher P- and N-contents in the MCA@PZS hybrid as well as the combined effect of MCA and PZS, which maximize the possible strong interactions between the PA6 matrix and the MCA@PZS hybrid in the PA6/MCA@PZS-5% composite.

On the basis of the above discussion of condensed-phase and gas-phase FR activities, the suitable FR mechanism of the PA6/MCA@PZS composite is schematically proposed in Figure 12. The MCA is functionalized with PZS to improve the FR properties of MCA nanosheets when they are dispersed in the PA6 matrix. During combustion, the volatile flammable gases, such as hydrocarbons, aromatic components, and other various small organic components escaped from the volatile PA6 composite to the flame zone as shown in Figure 12, which supports continuous combustion with the release of heat. However, the MCA@PZS hybrid containing composite exhibited a more efficient FR activity than the composites containing MCA or PZS solely. This is because of two reasons: first, the gas-phase flame-retardant activity of MCA improves the degradation process of MCA@PZS during combustion. The N element of MCA releases nonflammable gases and dilutes the oxygen concentration and it also absorbs the heat with endothermic degradation and cools the flame zone area. Second, the condensed phase flame-retardant effect of PZS on the surface of MCA, which increases the carbonaceous of polymer chains to form the thermally insulating char and thereby high compact and rigid protective layer is formed. This layer prevents the heat and mass transfer, and the escape of pyrolytic components in between the PA6 matrix and flame zone area results in decreasing both toxic smoke formation and heat release. Moreover, the increased loading of the MCA@PZS hybrid in the composite significantly improves the rheological property, which further supports the formation of polyaromatic P-N-containing high cross-linked components in the condensed phase and provides strong barrier properties.

3. CONCLUSIONS

In this work, the novel halogen-free supramolecular MCA@PZS hybrid was synthesized via a condensation polymerization method with MCA nanosheets as the template. This hybrid structure comprised high P- and N-contents with extensive cross-linkage, which improved the FR activity of the PA6 composites. Further, PA6 composites comprising the hybrid

FR MCA@PZS and individual FR MCA and PZS were also prepared and their flammability properties compared. The cone calorimetry test results revealed that the MCA@PZS hybrid containing composite improved the FR activity of the PA6 polymer, with lower HRR, THR, COP, and CO₂P values and toxic gas evolution during combustion over those afforded by individual MCA and PZS. The TG-FTIR and Py-GC-MS data revealed that the PA6/MCA@PZS-5% composites strongly inhibited the release of small organic volatile compounds, COP, and other toxicants, thereby implying a decrease in the smoke toxicity. Moreover, during thermal degradation, the combined effect of MCA and PZS allowed these composites to interact with the PA6 degraded components in different directions to form highly cross-linked dense char. This type of char can prevent heat and toxicant evolution and hence decreases the fire toxicity. The PA6 composites comprising the MCA@PZS hybrid achieved a V-0 rating in the UL-94 test, with a decrease in burning time and no melt drippings. Overall, this work illustrates that the synthesized MCA@PZS hybrid shows excellent potential as an FR additive in PA6 polymers to further extend the applications of this polymer.

4. EXPERIMENTAL SECTION

4.1. Materials. PA6 (1034B) was supplied by Ube Industries Ltd., Tokyo, Japan. HCCP, BPS, TEA, acetonitrile 98%, DMSO, melamine, and cyanuric acid were purchased from Sigma-Aldrich, Johannesburg, South Africa, and used as received without further purification.

4.2. Synthesis of MCA. MCA was synthesized according to a previously reported procedure,³⁶ with modification. Thus, equimolar ratios of melamine (1 g) and cyanuric acid (1.02 g) were dissolved separately in 40 and 20 mL DMSO, respectively, and then mixed together. The resultant white suspension, which formed immediately after mixing, was stirred continuously at 70 °C for 24 h. The afforded MCA was then centrifuged, washed twofold with distilled water and ethanol, and finally dried in a vacuum oven at 80 °C for 24 h.

4.3. Synthesis of PZS. HCCP (1.8 g, 5.18 mmol) and BPS (4.8 g, 19.2 mmol) were dissolved separately in 150 mL acetonitrile, mixed, and subsequently sonicated for 30 min at 25 °C. TEA (4.32 g, 42 mmol) was then added to the reaction mixture to immediately form a milky white suspension. The suspension was then sonicated at 50 °C for a further 4 h. The resultant white suspension was centrifuged, washed twofold

with distilled water and ethanol, and finally dried at 80 °C in a vacuum oven for 24 h.

4.4. Functionalization of the MCA@PZS Hybrid. The supramolecular halogen-free FR MCA@PZS was synthesized by PZS functionalization on the surface of planar MCA nanosheets via the sol–gel method. First, 2 g of synthesized MCA nanosheets were dispersed in 100 mL of acetonitrile and stirred for 30 min. Exactly 0.5 g of HCCP was then added and after complete dissolution, the mixture was stirred for a further 30 min; 4 mL of TEA was then added under continuous stirring. Next, the calculated weight of BPS dissolved in acetonitrile was added slowly to the reaction mixture, under stirring, across a period of 30 min and the mixture was stirred for a further 1 h. The resulting reaction mixture was further sonicated for 4 h to obtain a white suspension, which was washed twofold with distilled water and ethanol, and dried in a vacuum oven (80 °C for 24 h).

4.5. Preparation of the PA6 Composites. The PA6 composites were prepared by a melt blending method using different weight percentages of the MCA@PZS hybrid as well as individual MCA and PZS. Prior to extrusion, all the samples were dried in an oven at 80 °C for 24 h. A twin-screw extruder (process 11, co-rotating twin-screw extruder, $L/D = 40$, Thermo Scientific, USA) was employed and the extruded samples were collected via a water bath and subsequently pelletized. Different temperatures were maintained (128, 240, 250, 260, 260, 260, and 260 °C) at different zones during processing, whereas the dye temperature was 250 °C. The screw speed was maintained at 200 rpm, and the obtained samples in the extruder were further melt-blended and compression molded at 240 °C. All the samples were first melted at 240 °C for 5 min and a pressure of 1 Mton was then applied for 1 min. Next, the molded samples were cooled down to 24 °C using tap water, and the pressure was then released. The afforded samples were used for further characterization.

4.6. Characterization and Property Measurements. The XRD patterns of all the synthesized powder samples (MCA, PZS, and MCA@PZS) were collected from the X-ray generator using a PANalytical X'pert PRO diffractometer (The Netherlands) and Cu $K\alpha$ radiation ($\lambda = 0.154$ nm; current = 30 mA and voltage = 40 kV). The diffractograms were collected at a scan rate of 0.6/min at the 2θ range 2–80°. TGA (model TGA Q800, TA Instruments, USA) was performed in the temperature range 30–800 °C at a heating rate of 20 °C/min under a nitrogen/oxygen atmosphere. The microstructures of the char residues were elucidated by SEM (AURIGA Crossbeam Workstation, Carl Zeiss, Germany) at 3 kV. To evaluate the degradable volatile components of PA6 and its composites with different FR contents, TGA–FTIR–MS and Py–GC–MS were carried out using a PerkinElmer (USA) Pyris 1 TGA thermogravimetric analyzer connected to a Nicolet ISS0 spectrometer in the temperature range 50–800 °C, at a heating rate of 20 °C/min, under nitrogen. The tested PA6 composite samples weighed approximately 20 mg. XPS measurements of MCA and the MCA@PZS hybrid were conducted using a Kratos Axis Ultra device (Kratos, UK) with monochromatic (Al $K\alpha$) excitation source. The flammability properties of PA6 and its composites with different FR contents were studied by cone calorimetry (Fire Testing Technology, East Grinstead, UK) according to ISO 5660. The prepared test specimen samples (dimensions = 100 × 100 × 3 mm³) were wrapped in aluminum foil with the top surface open and exposed to the radiant cone at a heat flux of 25 kW/

m². The vertical burning test was carried out using an FTT (Fire Testing Technology), model UL-94, Fire Testing Technology Limited, U.K., according to the ASTM D5207 and the test specimen of 125 × 13 × 3.2 mm³ were prepared by the melt-compression method.

AUTHOR INFORMATION

Corresponding Author

*E-mail: rsuprakas@csir.co.za, ssinharay@uj.ac.za, suprakas73@yahoo.com. Phone: +27 12 841 2388. Website: www.csir.co.za/nano.

ORCID

Suprakas Sinha Ray: 0000-0002-0007-2595

Notes

The authors declare no competing financial interest.

ACKNOWLEDGMENTS

The authors would like to thank the Council for Scientific and Industrial Research (HGER74P) and Department of Science and Technology (HGERA8X) for financial support. The authors also thank Dr. Vincent Ojijo and Lesego Maubane for their help in the flammability test and TG–FTIR–Py–GC–MS analyses.

REFERENCES

- (1) Meng, H.; Sui, G. X.; Xie, G. Y.; Yang, R. Friction and wear behavior of carbon nanotubes reinforced polyamide 6 composites under dry sliding and water lubricated condition. *Compos. Sci. Technol.* **2009**, *69*, 606–611.
- (2) Yang, F.; Ou, Y.; Yu, Z. Polyamide 6/silica nanocomposites prepared by in situ polymerization. *J. Appl. Polym. Sci.* **1998**, *69*, 355–361.
- (3) Hu, Y.; Wang, S.; Ling, Z.; Zhuang, Y.; Chen, Z.; Fan, W. Preparation and combustion properties of flame retardant nylon 6/ montmorillonite nanocomposite. *Macromol. Mater. Eng.* **2003**, *288*, 272–276.
- (4) Liu, Y.; Wang, Q. The investigation on the flame retardancy mechanism of nitrogen flame retardant melamine cyanurate in polyamide 6. *J. Polym. Res.* **2009**, *16*, 583–589.
- (5) Wu, Z.-Y.; Xu, W.; Liu, Y.-C.; Xia, J.-K.; Wu, Q.-X.; Xu, W.-J. Preparation and characterization of flame-retardant melamine cyanurate/polyamide 6 nanocomposites by in situ polymerization. *J. Appl. Polym. Sci.* **2009**, *113*, 2109–2116.
- (6) Balabanovich, A. I.; Schnabel, W. Fire Retardance in Polyamide-6,6. The Effects of Red Phosphorus and Radiation-Induced Cross-Links. *Macromol. Mater. Eng.* **2002**, *287*, 187–194.
- (7) Liu, H.; Wang, X.; Wu, D. Novel cyclotriphosphazene-based epoxy compound and its application in halogen-free epoxy thermosetting systems: Synthesis, curing behaviors, and flame retardancy. *Polym. Degrad. Stab.* **2014**, *103*, 96–112.
- (8) Jin, W.; Yuan, L.; Liang, G.; Gu, A. Multifunctional Cyclotriphosphazene/Hexagonal Boron Nitride Hybrids and Their Flame Retarding Bismaleimide Resins with High Thermal Conductivity and Thermal Stability. *ACS Appl. Mater. Interfaces* **2014**, *6*, 14931–14944.
- (9) Tsubota, T.; Morita, M.; Murakami, N.; Ohno, T. Performance of carbon material derived from starch mixed with flame retardant as electrochemical capacitor. *J. Power Sources* **2014**, *267*, 635–640.
- (10) Chen, X.; Jiang, Y.; Jiao, C. Smoke suppression properties of ferrite yellow on flame retardant thermoplastic polyurethane based on ammonium polyphosphate. *J. Hazard. Mater.* **2014**, *266*, 114–121.
- (11) Bielejewski, A. G.; Marjo, C. E.; Prins, L. J.; Timmerman, P.; de Jong, F.; Reinhoudt, D. N. Thermodynamic Stabilities of Linear and Crinkled Tapes and Cyclic Rosettes in Melamine–Cyanurate Assemblies: A Model Description. *J. Am. Chem. Soc.* **2001**, *123*, 7518–7533.

- (12) Tao, W.; Li, J. Melamine Cyanurate Tailored by Base and Its Multi Effects on Flame Retardancy of Polyamide 6. *Appl. Surf. Sci.* **2018**, *456*, 751–762.
- (13) Malkappa, K.; Ray, S. S.; Kumar, N. Enhanced Thermo-Mechanical Stiffness, Thermal Stability, and Fire Retardant Performance of Surface-Modified 2D MoS₂ Nanosheet-Reinforced Polyurethane Composites. *Macromol. Mater. Eng.* **2019**, *304*, 1800562.
- (14) Malkappa, K.; Bandyopadhyay, J.; Ray, S. Thermal degradation characteristic and flame retardancy of polylactide-based nanobiocomposites. *Molecules* **2018**, *23*, 2648.
- (15) Feng, X.; Wang, X.; Cai, W.; Hong, N.; Hu, Y.; Liew, K. M. Integrated effect of supramolecular self-assembled sandwich-like melamine cyanurate/MoS₂ hybrid sheets on reducing fire hazards of polyamide 6 composites. *J. Hazard. Mater.* **2016**, *320*, 252–264.
- (16) Gao, F.; Tong, L.; Fang, Z. Effect of a novel phosphorous-nitrogen containing intumescent flame retardant on the fire retardancy and the thermal behaviour of poly(butylene terephthalate). *Polym. Degrad. Stab.* **2006**, *91*, 1295–1299.
- (17) Xiao, J.; Hu, Y.; Yang, L.; Cai, Y.; Song, L.; Chen, Z.; Fan, W. Fire retardant synergism between melamine and triphenyl phosphate in poly(butylene terephthalate). *Polym. Degrad. Stab.* **2006**, *91*, 2093–2100.
- (18) Shen, D.; Xu, Y.-J.; Long, J.-W.; Shi, X.-H.; Chen, L.; Wang, Y.-Z. Epoxy resin flame-retarded via a novel melamine-organophosphinic acid salt: Thermal stability, flame retardance and pyrolysis behavior. *J. Anal. Appl. Pyrolysis* **2017**, *128*, 54–63.
- (19) Chen, Y.; Wang, W.; Qiu, Y.; Li, L.; Qian, L.; Xin, F. Terminal group effects of phosphazene-triazine bi-group flame retardant additives in flame retardant polylactic acid composites. *Polym. Degrad. Stab.* **2017**, *140*, 166–175.
- (20) Ke, C.-H.; Li, J.; Fang, K.-Y.; Zhu, Q.-L.; Zhu, J.; Yan, Q.; Wang, Y.-Z.; Yan, Q.; Wang, Y. Z. Synergistic effect between a novel hyperbranched charring agent and ammonium polyphosphate on the flame retardant and anti-dripping properties of polylactide. *Polym. Degrad. Stab.* **2010**, *95*, 763–770.
- (21) Zhao, D.; Wang, J.; Wang, X.-L.; Wang, Y.-Z. Highly thermostable and durably flame-retardant unsaturated polyester modified by a novel polymeric flame retardant containing Schiff base and spirocyclic structures. *Chem. Eng. J.* **2018**, *344*, 419–430.
- (22) Liu, W.; Huang, X.; Wei, H.; Tang, X.; Zhu, L. Intrinsically fluorescent nanoparticles with excellent stability based on a highly crosslinked organic-inorganic hybrid polyphosphazene material. *Chem. Commun.* **2011**, *47*, 11447–11449.
- (23) Wang, X.; Fu, J.; Wang, M.; Wang, Y.; Chen, Z.; Zhang, J.; Chen, J.; Xu, Q. Facile synthesis of Au nanoparticles supported on polyphosphazene functionalized carbon nanotubes for catalytic reduction of 4-nitrophenol. *J. Mater. Sci.* **2014**, *49*, 5056–5065.
- (24) Qu, T.; Yang, N.; Hou, J.; Li, G.; Yao, Y.; Zhang, Q.; He, L.; Wu, D.; Qu, X. Flame retarding epoxy composites with poly-(phosphazene-co-bisphenol A)-coated boron nitride to improve thermal conductivity and thermal stability. *RSC Adv.* **2017**, *7*, 6140–6151.
- (25) Qiu, S.; Xing, W.; Feng, X.; Yu, B.; Mu, X.; Yuen, R. K. K.; Hu, Y. Self-standing cuprous oxide nanoparticles on silica@ polyphosphazene nanospheres: 3D nanostructure for enhancing the flame retardancy and toxic effluents elimination of epoxy resins via synergistic catalytic effect. *Chem. Eng. J.* **2017**, *309*, 802–814.
- (26) Qiu, S.; Xing, W.; Mu, X.; Feng, X.; Ma, C.; Yuen, R. K. K.; Hu, Y. A 3D nanostructure based on transition-metal phosphide decorated heteroatom-doped mesoporous nanospheres interconnected with graphene: Synthesis and applications. *ACS Appl. Mater. Interfaces* **2016**, *8*, 32528–32540.
- (27) Fu, J.; Huang, X.; Huang, Y.; Zhang, J.; Tang, X. One-pot noncovalent method to functionalize multi-walled carbon nanotubes using cyclomatrix-type polyphosphazenes. *Chem. Commun.* **2009**, *9*, 1049–1051.
- (28) Fu, J.; Xu, Q.; Chen, J.; Chen, Z.; Huang, X.; Tang, X. Controlled fabrication of uniform hollow core porous shell carbon spheres by the pyrolysis of core/shell polystyrene/cross-linked polyphosphazene composites. *Chem. Commun.* **2010**, *46*, 6563–6565.
- (29) Luther, T. A.; Stewart, F. F.; Lash, R. P.; Wey, J. E.; Harrup, M. K. Synthesis and characterization of poly{hexakis[(methyl)(4-hydroxyphenoxy)]cyclo-triphosphazene}. *J. Appl. Polym. Sci.* **2001**, *82*, 3439–3446.
- (30) Zhu, Y.; Huang, X.; Li, W.; Fu, J.; Tang, X. Preparation of novel hybrid inorganic-organic microspheres with active hydroxyl groups using ultrasonic irradiation via one-step precipitation polymerization. *Mater. Lett.* **2008**, *62*, 1389–1392.
- (31) Wei, W.; Huang, X.; Zhao, X.; Zhang, P.; Tang, X. A rapid and efficient strategy for preparation of super-hydrophobic surface with cross-linked cyclotriphosphazene/6F-bisphenol A copolymer microspheres. *Chem. Commun.* **2010**, *46*, 487–489.
- (32) Liu, W.; Huang, X.; Wei, H.; Chen, K.; Gao, J.; Tang, X. Facile preparation of hollow crosslinked polyphosphazene submicrospheres with mesoporous shells. *J. Mater. Chem.* **2011**, *21*, 12964–12968.
- (33) Huang, X.; Wei, W.; Zhao, X.; Tang, X. Novel preparation of polyphosphazene-coated carbon nanotubes as a Pt catalyst support. *Chem. Commun.* **2010**, *46*, 8848–8850.
- (34) Hu, Y.; Meng, L.; Niu, L.; Lu, Q. Facile Synthesis of Superparamagnetic Fe₃O₄@polyphosphazene@Au Shells for Magnetic Resonance Imaging and Photothermal Therapy. *ACS Appl. Mater. Interfaces* **2013**, *5*, 4586–4591.
- (35) Fu, J.; Huang, X.; Huang, Y.; Pan, Y.; Zhu, Y.; Tang, X. Preparation of Silver Nanocables Wrapped with Highly Cross-Linked Organic-Inorganic Hybrid Polyphosphazenes via a Hard-Template Approach. *J. Phys. Chem. C* **2008**, *112*, 16840–16844.
- (36) Huang, H.; Zhang, K.; Jiang, J.; Li, J.; Liu, Y. Highly dispersed melamine cyanurate flame-retardant epoxy resin composites. *Polym. Int.* **2017**, *66*, 85–91.
- (37) Qiu, S.; Ma, C.; Wang, X.; Zhou, X.; Feng, X.; Yuen, R. K. K.; Hu, Y. Melamine-containing polyphosphazene wrapped ammonium polyphosphate: A novel multifunctional organic-inorganic hybrid flame retardant. *J. Hazard. Mater.* **2018**, *344*, 839–848.
- (38) Zhou, X.; Qiu, S.; Xing, W.; Gangireddy, C. S. R.; Gui, Z.; Hu, Y. Hierarchical Polyphosphazene@Molybdenum Disulfide Hybrid Structure for Enhancing the Flame Retardancy and Mechanical Property of Epoxy Resins. *ACS Appl. Mater. Interfaces* **2017**, *9*, 29147–29156.
- (39) Yang, W.; Yang, F.; Yang, R.; Wang, B. Ammonium Polyphosphate/Melamine Cyanurate Synergetic Flame Retardant System for Use in Papermaking. *BioResources* **2016**, *11*, 2308–2318.
- (40) Jing, J.; Zhang, Y.; Tang, X.; Zhou, Y.; Li, X.; Kandola, B. K.; Fang, Z. Layer by layer deposition of polyethylenimine and bio-based polyphosphate on ammonium polyphosphate: A novel hybrid for simultaneously improving the flame retardancy and toughness of polylactic acid. *Polymer* **2017**, *108*, 361–371.
- (41) Bourbigot, S.; Le Bras, M.; Delobel, R.; Gengembre, L. XPS study of an intumescent coating. *Appl. Surf. Sci.* **1997**, *120*, 15–29.
- (42) Liang, W.-j.; Zhao, B.; Zhao, P.-h.; Zhang, C.-y.; Liu, Y.-q. Bisphenol-S bridged penta(anilino)cyclotriphosphazene and its application in epoxy resins: Synthesis, thermal degradation, and flame retardancy. *Polym. Degrad. Stab.* **2017**, *135*, 140–151.
- (43) Yu, B.; Shi, Y.; Yuan, B.; Qiu, S.; Xing, W.; Hu, W.; Song, L.; Lo, S.; Hu, Y. Enhanced thermal and flame retardant properties of flame-retardant-wrapped graphene/epoxy resin nanocomposites. *J. Mater. Chem. A* **2015**, *3*, 8034–8044.
- (44) Levchik, S. V.; Weil, E. D.; Lewin, M. Thermal decomposition of aliphatic nylons. *Polym. Int.* **1999**, *48*, 532–557.
- (45) Ramani, A.; Dahoe, A. E. On flame retardancy in polycaprolactam composites by aluminum diethylphosphinate and melamine polyphosphate in conjunction with organically modified montmorillonite nanoclay. *Polym. Degrad. Stab.* **2014**, *105*, 1–11.
- (46) Wang, P.; Cai, Z. Highly efficient flame-retardant epoxy resin with a novel DOPO-based triazole compound: Thermal stability, flame retardancy and mechanism. *Polym. Degrad. Stab.* **2017**, *137*, 138–150.

(47) Zhang, X.; Zhong, Y.; Mao, Z.-P. The flame retardancy and thermal stability properties of poly (ethylene terephthalate)/hexakis (4-nitrophenoxy) cyclotriphosphazene systems. *Polym. Degrad. Stab.* **2012**, *97*, 1504–1510.

(48) Chen, M.-J.; Xu, Y.-J.; Rao, W.-H.; Huang, J.-Q.; Wang, X.-L.; Chen, L.; Wang, Y.-Z. Influence of valence and structure of phosphorus-containing melamine salts on the decomposition and fire behaviors of flexible polyurethane foams. *Ind. Eng. Chem. Res.* **2014**, *53*, 8773–8783.

(49) Rao, W.-H.; Hu, Z.-Y.; Xu, H.-X.; Xu, Y.-J.; Qi, M.; Liao, W. -retardant flexible polyurethane foams with highly efficient melamine salt. *Ind. Eng. Chem. Res.* **2017**, *56*, 7112–7119.

(50) Ramani, A.; Dahoe, A. E. On flame retardancy in polycaprolactam composites by aluminium diethylphosphinate and melamine polyphosphate in conjunction with organically modified montmorillonite nanoclay. *Polym. Degrad. Stab.* **2014**, *105*, 1–11.

(51) Salehiyan, R.; Malwela, T.; Ray, S. S. Thermo-oxidative degradation study of melt-processed polyethylene and its blend with polyamide using time-resolved rheometry. *Polym. Degrad. Stab.* **2017**, *139*, 130–137.